PHYSICAL REVIEW C VOLUME 24, NUMBER 2 AUGUST 1981

Feedback of giant resonances on optical model potentials

M. Pignanelli* and H. V. von Geramb
Universität Hamburg, Luruper Chaussee 149, D-2000 Hamburg 50, West Germany

R. De Leo
Istituto di Fisica dell'Università and Istituto Nazionale di Fisica Nucleare, Sezione di Bari, Bari, Italy

(Received 18 July 1980)

A nuclear structure effect in $A < 70$ nuclei for elastic proton scattering, $25 < E < 50$ MeV, is identified with a strong channel coupling to known giant multipole resonances. Numerical studies reveal it as an effective l-dependent absorptive and repulsive optical model contribution. For an understanding in terms of microscopic optical potentials the connection between Brueckner-Hartree-Fock and nuclear structure approaches is discussed.

[NUCLEAR REACTIONS Proton elastic scattering on ^{16,18}O, ^{24}Mg, ^{40}Ar, and ^{40}Ca, $E_p = 21-48$ MeV. Comparisons with optical model and coupled channel calculations. Deduced coupling strengths.]

I. INTRODUCTION

Recent systematic measurements gave evidence for nuclear structure effects in proton elastic scattering on light and medium mass nuclei.[1,2] They consist of an enhancement of differential cross sections at backward angles with $\theta > 120°$ and projectile energies between 25 and 50 MeV. The effect, which is not a diffractionlike phenomenon, consists of a maximum whose angular position is energy independent. Experimentally observed, the maximum is pronounced for closed shell nuclei such as ^{16}O and ^{40}Ca, while it is less evident for deformed nuclei.

It is well established that standard phenomenological optical model potentials (OMP),[1-5] as well as microscopic OMP's,[6,7] fail to account for the observed effect. Attempts with nonstandard radial form factors[8] improved the fit at some energies but left others unaltered.[1] Alternatively, strong evidence has been collected for l-dependent effects.[9] With intensive efforts Kobos and Mackintosh[10] have collected evidence for l-dependent terms in OMP's with the result of perfect fits in the full angular range. An explicit coupling of the deuteron channel to the elastic channel[11] has been considered by these authors as the main cause of the l dependence. The calculation was performed by including proton and deuteron coupled reaction channels (CRC) in addition to an optical model foreground amplitude. To reproduce the experimental data the OMP's were refitted and thereby drastically changed.[11]

The many-body formulation and evaluation of microscopic OMP's has been considered in several recent studies. Of particular interest here is the Brueckner-Hartree-Fock (BHF) potential which sums up the two particle ladder diagrams[6,7] and the nuclear structure approach,[12] which sums up the particle-hole bubble diagrams. As such, the last approach takes into account two-step processes with excitations of collective target states. Both approaches yield a nonlocal and energy dependent optical potential.

BHF is calculated in infinite nuclear matter with a free nucleon-nucleon potential as input, and the Pauli principle is included. Since this approach includes an exact treatment of particle-particle correlations in its summation of ladder diagrams, the proton-neutron correlations, the deuteron as a particularity, are fully included.[6,7] The effects of the deuteron channel, which is claimed by other authors[11] to yield shell effects, does not have any prominent role in BHF and is one of many contributions to a smoothly varying potential. This should not weaken the importance of the deuteron channel as a source of the imaginary potential but we claim rather that the smooth phenomenological OMP contains the deuteron channel equally well as the BHF results do.

The nuclear structure OMP is designed for finite nuclei.[12] The leading term is the real Hartree-Fock potential with l-dependent corrections coming from a resummation of all bubble diagrams. The intermediate channels correspond to excitations of the target nucleus, described in the random phase approximation (RPA). It has already been pointed out by Vinh Mau that the two approaches are complementary in the sense that the nuclear matter approach should be more adequate for projectile energies in a range where collective states are present, i.e., the giant dipole and

quadrupole resonance region.[13,14] On the other hand, the BHF approach should be more adequate at higher energies.

The present study is devoted to relating these approaches for microscopic OMP's with a new analysis and physical interpretation of nuclear structure effects seen in proton elastic scattering from light nuclei.

II. THEORETICAL BACKGROUND

Microscopic optical potentials are related to the mass operator or generalized optical model. The different computations distinguish essentially the contributions shown in Fig. 1 as important ingredients. In BHF, Fig. 1(a), the ladder diagram summation is contained in the dashed line which represents a complex energy and density dependent effective interaction or reaction matrix. The nonlocal complex OMP is the result of an antisymmetrized folding procedure with the diagonal and nondiagonal single particle density of the target ground state. The imaginary OMP represents loss of flux into a homogeneous excitation spectrum.[6,7] The incorporation and resummation of

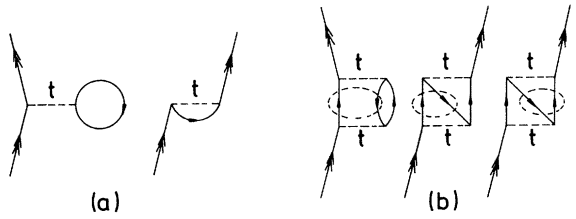

FIG. 1. Leading terms in the microscopic optical potential: (a) direct and exchange potentials of the lowest order BHF with the summed ladder diagrams of the N-N interaction; (b) direct and exchange particle-hole correlation included in a resummation of bubble diagrams in the nuclear structure approach of the optical model potential.

bubble diagrams,[12] Fig. 1(b), enables one to account for intermediate channels corresponding to excitations of the target nucleus states described in RPA. This permits one to account for shell effects and collective phenomena in specific nuclei and to overcome possible shortcomings of the calculations restricted to graphs in Fig. 1(a). One can therefore combine the BHF with the nuclear structure contributions and use

$$U(\vec{r},\vec{r}',E)=\delta(\vec{r}-\vec{r}')\int d^3r''\rho_{00}(\vec{r}'')t(\vec{r},\vec{r}'',E)-\rho_{00}(\vec{r},\vec{r}')t(\vec{r},\vec{r}',E)$$

$$+\sum_{n\neq 0}\frac{\int d^3r''\rho_{0n}(\vec{r}'')t(\vec{r},\vec{r}'',E)\Psi_n(\vec{r})\Psi_n^*(\vec{r}')\int d^3r''\rho_{n0}(\vec{r}'')t(\vec{r}'',\vec{r}',E)}{E-E_n-\epsilon_n+i\delta}\,.$$

The first two terms obtain their smooth (and small) energy dependence from the complex effective interaction $t(\vec{r},\vec{r}',E)$. Their behavior shows little structure sensitivity and does not distinguish light and heavy nucleus particularities despite their densities.

The last term is a correction and represents structural deficiencies in BHF, in particular the neglect of particle-hole correlations appearing as low-lying collective states or high-lying giant multipole resonances in finite nuclei. This potential is nonlocal and strongly energy dependent due to the energy denominator. Furthermore, this potential, with its structural ingredients coming from a limited number of explicitly treated states, is l dependent and is characterized by matching and mismatching conditions in transition amplitudes. To take into account the contributions coming from this term, we treat the whole as a coupled channel problem. As a first step a series of model calculations are given based on BHF real, imaginary, central, and spin-orbit potentials. The incorporation of collective states and the structural consequences are studied for ^{16}O, ^{40}Ca, and ^{90}Zr, with their results given in Figs. 2 and 3. ^{16}O and ^{40}Ca are exemplary nuclei with strong back angle features, whereas ^{90}Zr lies beyond this region and BHF yields a good approximation for realistic OMP's.

The nucleus considered in the calculations of Fig. 2 is ^{40}Ca. The intermediate quadrupole state is described as a vibrational one-phonon state located at 18.5 MeV. In the calculation the collective transition form factors have been obtained by deforming a potential which corresponds to the average of the potentials for the elastic and inelastic channels. The curves reported are for deformations $\beta_2=0$ (no coupling), 0.17 [40% of the linear energy weighted sum rule (EWSR) limit] and 0.23 (75% EWSR). By increasing the coupling strength the structural changes in the angular distribution at backward angles exhibit a deep minimum at 135° and a peak around 160°. In this calculation we find the excitation energy of the inter-

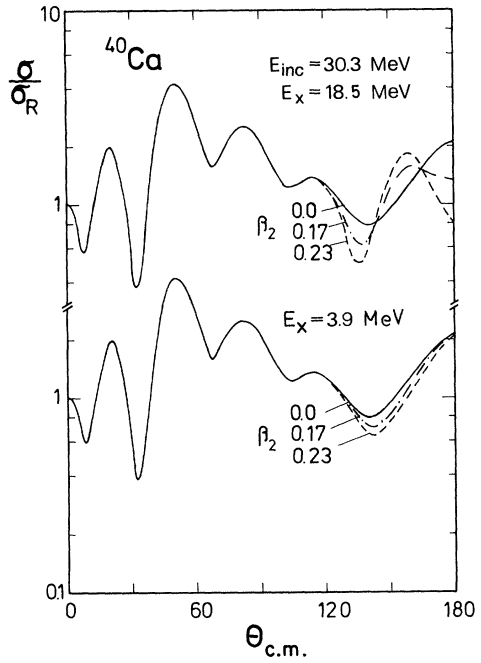

FIG. 2. Theoretical model studies of the influence of a giant quadrupole resonance, $E_x = 18.5$ MeV, exhausting 0%, 40%, and 75% of the EWSR limit, $\beta_2 = 0$, 0.17, and 0.23, respectively. In the lower part the same β_2 values were used when coupling a low-lying 2^+ state.

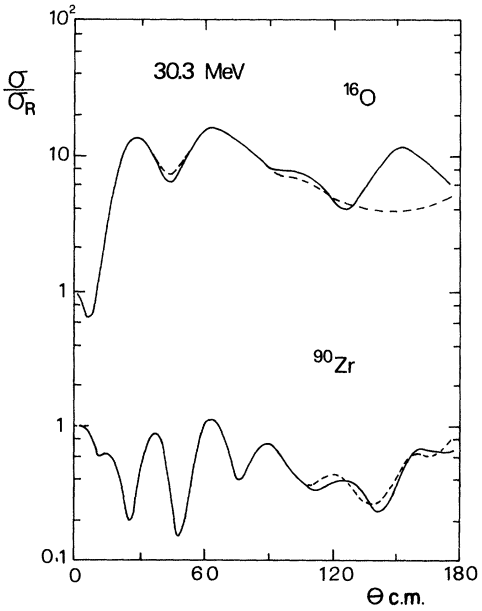

FIG. 3. Model studies for ^{16}O and ^{90}Zr showing the mass dependence of the effect obtained from the coupling with a quadrupole state lying in the giant resonance region. The dashed lines are proton elastic cross sections with no coupling, while the continuous lines are for a coupling equivalent to 100% of the EWSR limit.

mediate state to be important since it determines the opening or closing of the channel. In transitions to giant resonance (GR) states the channel flux is very limited and receives less than 1% of the total reaction cross section. The flux is redistributed into other angular regions in the elastic channel. To emphasize these features we display in the lower half of Fig. 2 similar angular distributions, but with the quadrupole state positioned at 3.9 MeV, as experimentally found for the lowest 2^+ state in ^{40}Ca. The elastic cross sections are now all similar, being only slightly altered in magnitude at backward angles. The inelastic cross section is now large (> 10 mb); the loss of flux more significant, and the effect in the elastic cross section can be simply reproduced by an increment in the imaginary term of the OMP.

To show the average mass dependence of the observed effect, calculations for ^{16}O and ^{90}Zr are shown in Fig. 3. The quadrupole intermediate state has been positioned at 22 and 14.5 MeV, according to experimental giant quadrupole resonance (GQR) centroids. The 100% EWSR limit has been assumed in both cases: $\beta_2 = 0.518$ and 0.151, respectively. The effect is most obvious for the lighter nucleus and we attribute this to better matching conditions occurring in the case of a quadrupole state positioned above 20 MeV as for the lighter nucleus. Another reason is that for a given percentage of the EWSR the ratio of the inelastic to elastic cross section decreases when the mass increases.

In Refs. 5 and 6, by extensive comparisons, it has been shown that BHF potentials, in order to reproduce experimental angular distributions, need some renormalization in their strengths that may be as large as 10–20%. This procedure gives improved fits to forward angles but leaves substantially unaltered the disagreement at backward angles for nuclei such as ^{16}O and ^{40}Ca. The changes needed to reproduce the experiment in the latter angular region are of the type shown in Figs. 2 and 3 and can be produced by collective couplings. These couplings, as mentioned above, are *a priori* not included in BHF potentials.

To have quantitative information on coupling to GR states, instead of using BHF potentials and considering their strengths as free parameters, we found it more straightforward to use average phenomenological OMP's obtained from forward angle data at several incident energies without any further change. One may consider BHF and average phenomenological potentials as equivalent in several aspects. Interesting for the present study is the failure of both in reproducing detailed nuclear effects.

III. ANALYSIS OF CROSS SECTION AND POLARIZATION DATA

Proton elastic scattering experiments have recently been gathered and systematically studied with respect to deficiencies of a standard optical model analysis.[1,2] From a first inspection of differential cross sections the nuclei were classified into two groups. In the first we can find ^{12}C, ^{20,22}Ne, ^{24,26}Mg, and ^{28}Si, for which, in spite of noticeable fluctuations at low energies, the differential cross sections gradually assume a "standard" shape with increasing incident energy. Standard refers to a shape which is fitted by means of an optical model potential with standard and energy averaged geometries and well depths. In the second group of nuclei significant discrepancies remain. Well known are the difficulties found in fitting ^{16}O and ^{40}Ca. These difficulties are shown in an early paper by Gross *et al.*[3] and are mostly connected to the shape of differential cross sections at backward angles. A similar situation is found for other nuclei neighboring the shell closures such as ^{14,15}N, ^{17,18}O, ^{35,37}Cl, and ^{40}Ar. Standard OMP's can reproduce total reaction cross sections well and polarization data and elastic cross sections at forward angles very satisfactorily, but fail to reproduce backward angles at incident energies between 25 and 50 MeV.

We concentrate on proton scattering from ^{40}Ca and from some other exemplary nuclei. ^{40}Ca data are considered at incident energies: 21.0, 26.3, 30.3, 35.8, 40.0, 45.5, and 48.0 MeV. Experimental studies[16] on the GQR in ^{40}Ca find 30—75 % of the EWSR exhausted in an energy interval between 16 and 22 MeV. The solid lines of Fig. 4 are from a coupled channel calculation (CC) with a 2^+ state at 18.5 MeV and using a coupling parameter $\beta_2 = 0.23$, 75% EWSR limit. The best fit optical model (OM) parameters given by van Oers (Table I of Ref. 5) have been used. For the inelastic channel and outgoing energies below 20 MeV the average set 1, given in Table I, has been derived. In this case and for the other nuclei considered below the same procedure was followed. Fixed values have been used for the geometrical parameters, while an average energy dependence has been assumed for the well depths. For the real well the energy dependence determined at higher energies has been used also below 20 MeV. The imaginary surface term has been taken increasing linearly with the energy from a negative energy, corresponding to the incoming proton binding energy up to about 20 MeV. Set 1 has been obtained from the fixed geometry potential of Ref. 5.

The cross sections at 21.0 MeV are well reproduced by an OM calculation (dashed line), while the collective coupling gives a small worsening of the fit. At this energy the effect can be easily compensated by an adjustment of some OM parameters. The same result is obtained at lower incident energies. At higher energies a worsening of the fits with simple OM calculations be-

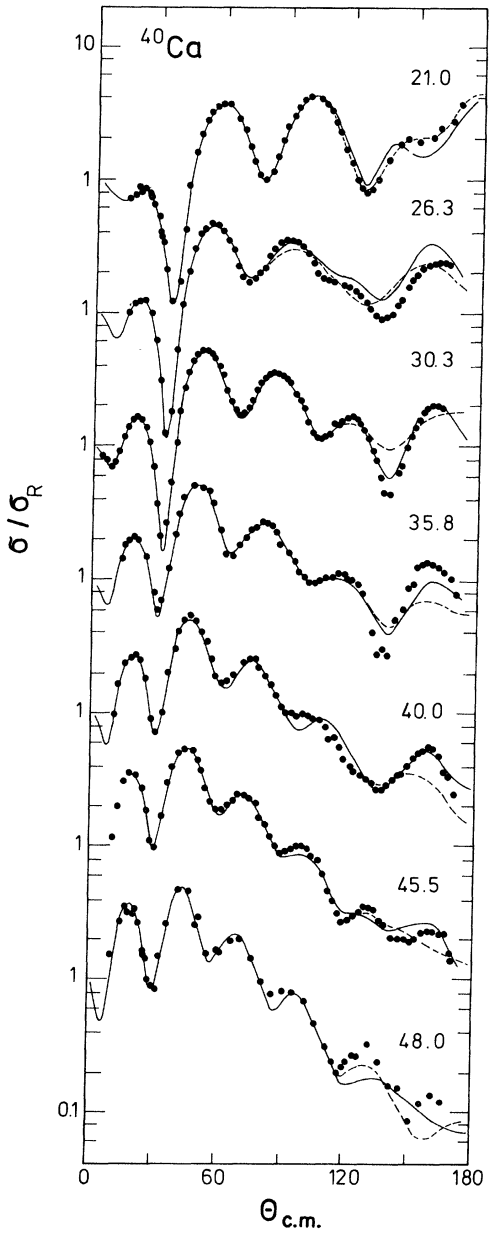

FIG. 4. Comparison of ^{40}Ca experimental data (Refs. 3,5) with theoretical angular distributions. The numbers given on the right are the incident energies in MeV. Theoretical curves are from OM calculations with the best fit parameters of Ref. 5 (dashed lines) and from CC calculations containing the coupling of a quadrupole state positioned at 18.5 MeV with a coupling strength $\beta_2 = 0.23$.

TABLE I. Average energy-dependent optical model parameters used in OM and CC calculations. The potentials are of the type

$$V(r) = -V_0 f(x_0) - iWf(x_w) + 4iW_D (d/dx_w) f(x_w) + V_C(r, R_C) + V_{so}(\hbar/m_\pi c)^2 (1/r)(d/dr) f(x_{so}),$$

where $f(x_i)$ are Woods-Saxon form factors with $x_i = (r - R_i A^{1/3})/a_i$ and V_C is the Coulomb potential of a uniformly charged sphere of radius $1.2A^{1/3}$.

Set	Nucleus	E_{inc} (MeV)	V_0 (MeV)	R_0 (fm)	a_0 (fm)	W (MeV)	W_D (MeV)	R_w (fm)	a_w (fm)	V_{so} (MeV)	R_{so} (fm)	a_{so} (fm)
1[a]	^{40}Ca	<20	b	1.152	0.692	0	$0.38 + 0.35E$	1.309	0.549	4.76	1.014	0.526
2	^{40}Ca	<21	$56.2 - 0.31E$	1.180	0.700	0	$0.31 + 0.29E$	1.300	0.600	5.89	1.050	0.700
		>21				$0.10E - 2.1$	$7.40 - 0.05E$					
3	^{40}Ca	<26	$58.0 - 0.31E$	1.145	0.750	$0.079E$	$0.23 + 0.21E$	1.142	0.465	6.60	0.967	0.742
		>26					$8.91 - 0.12E$					
4	^{40}Ar	<21	$59.1 - 0.30E$	1.140	0.750	0	$1.80 + 0.23E$	1.300	0.660	4.45	1.010	0.560
		>21				$0.23 - 4.4$	$10.0 - 0.156E$					
5	^{16}O	<20	$57.4 - 0.32E$	1.100	0.700	0	$1.10 + 0.15E$	1.300	0.670	6.00	1.000	0.600
		>20					4.1					
6	^{18}O	<15	$59.5 - 0.29E$	1.100	0.700	0	$1.70 + 0.22E$	1.300	0.670	6.00	1.000	0.600
		15–25				0	6.13					
		>25				$0.30E - 7.5$	$10.4 - 0.17E$					
7	^{24}Mg	<15	$55.9 - 0.30E$	1.144	0.690	0	$0.88 + 0.39E$	1.320	0.657	5.90	1.010	0.600
		15 – 22				0	$5.6 + 0.073E$					
		>22				$0.31E - 8.8$	$11.2 - 0.18E$					

[a] The imaginary surface term has a Gaussian form factor with a diffuseness $b = 2.11a_w$.

[b] $V_0 = 60.91 - 0.447E + 0.000\,841E^2$ as in Ref. 5.

comes evident. From 26.3 to 45.5 MeV the improvement obtained in CC calculations is also evident. It is stressed that this improvement is in comparison to a best fit calculation and without any further readjustment of OM parameters. The coupling is less effective at 48.0 MeV.

To display the role of the OMP's and collective couplings different sets of parameters were tried. Two average potentials are given in Table I as sets 2 and 3. Set 2 was obtained in previous studies[1,3] by fitting forward angle data, while set 3 has been obtained by averaging the best fit parameters of Ref. 5 for incident energies larger than 30 MeV. These two potentials are nearly equivalent when used in OM calculations, while in CC calculations the better results are obtained with set 2 below 30 MeV and with set 3 above. Set 2, displaying a radius larger for the real well and smaller for the imaginary well, should be more appropriate than set 3 at low energies. This result is in qualitative agreement with BHF predictions. For the curves given in Fig. 5, set 2 has been used at 21.0, 26.3, and 30.3 MeV and set 3 at other energies. The coupling with the GQR gives an agreement with the experimental differential cross sections up to 30.3 MeV. At higher energies, whichever OMP is used, the calculated cross sections are less sensitive to a quadrupole state positioned around 20 MeV. A larger coupling strength (100% of EWSR or more) can still produce acceptable fits at 35.8 and 40.0 MeV but not at 45.5 and 48.0 MeV. The long-dashed curves given in Fig. 5 for 40.0 and 45.5 MeV data have been obtained with $\beta_2 = 0.27$ (100% EWSR). On the other hand, the agreement with the experiment cannot be improved by considering minor components of the GQR lying at excitation energies larger than 22 MeV or the isovector dipole resonance, which is known to be located between 16 and 22 MeV, as the main part of the GQR.[17] A further marked improvement can be obtained by coupling with an octupole state lying in the 30–40 MeV excitation energy region. In the absence of detailed experimental information about $E3$ resonances, we can refer to RPA calculations,[18] which predict a broad distribution with the main part of the strength lying at energies above 30 MeV. We adopt $E_x = 120A^{1/3}$, which gives for the $E3$ centroid an excitation energy of 35 MeV. Introducing this coupling, the solid curves of Fig. 5 are obtained. The coupling strengths needed to fit the experiments are given in Table II. The EWSR exhausted is around 60% for the $E2$ and 15–20% for the $E3$ resonance.

The effect on the polarizations is shown in Figs. 6 and 7. The CC calculations give fits of a quality at least equivalent to that obtained by OM calculations, and very often the effect of the coupling with GR states is negligible. This is a further indication supporting the process studied here. It seems, in fact, phenomenologically established that nonstandard effects concern mainly the differential cross sections.

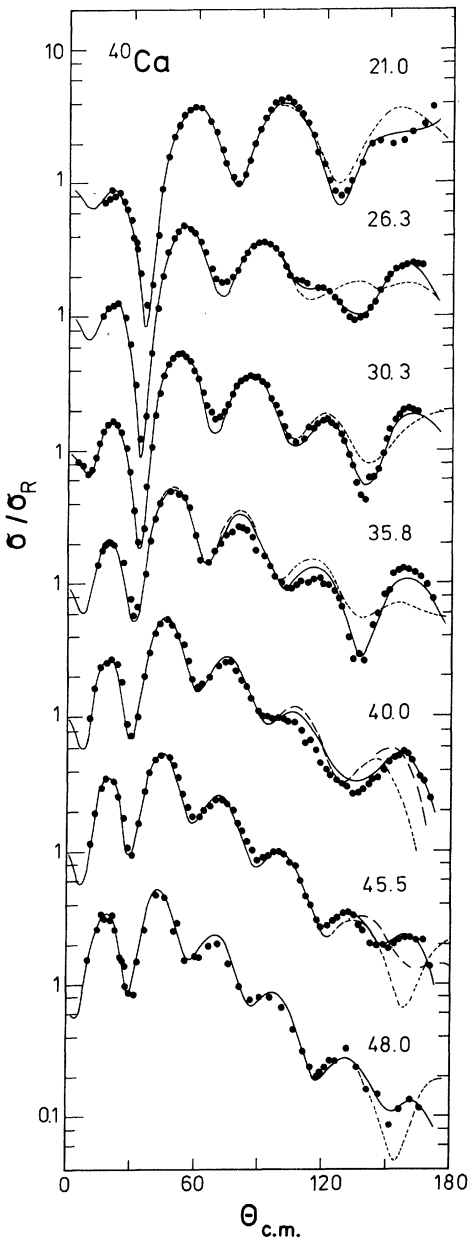

FIG. 5. Comparison of ^{40}Ca data with OM calculations using the average parameters of Table I (dashed lines). The solid lines give the effect of the coupling of quadrupole and octupole resonances to the ground state. The coupling parameters are listed in Table II. The long-dashed lines given at 40.0 and 45.5 MeV are obtained using the coupling with the quadrupole resonance only and the 100% EWSR limit.

TABLE II. Coupling strengths used in CC calculations for ^{40}Ca. The same deformation length $R\beta$ has been used for the different terms in the optical model potential. The EWSR limit has been evaluated using the radial distribution of the real central term.

E_{inc} (MeV)	β_2	β_3	$E2$ ($T=0$) % EWSR	$E3$ ($T=0$) % EWSR
21.0	0.19		50	
26.3	0.22		68	
30.3	0.20		56	
35.8	0.23	0.10	70	12
40.0	0.19	0.12	48	17
45.5	0.22	0.13	64	20
48.0	0.20	0.12	53	17

Similar calculations have been performed for several other nuclei in an attempt to obtain an explanation of the nuclear structure dependence of proton elastic scattering on light nuclei. We simply assume that this dependence comes from the structure of the giant resonances coupled with the ground state—its centroid energy, width, and strength.

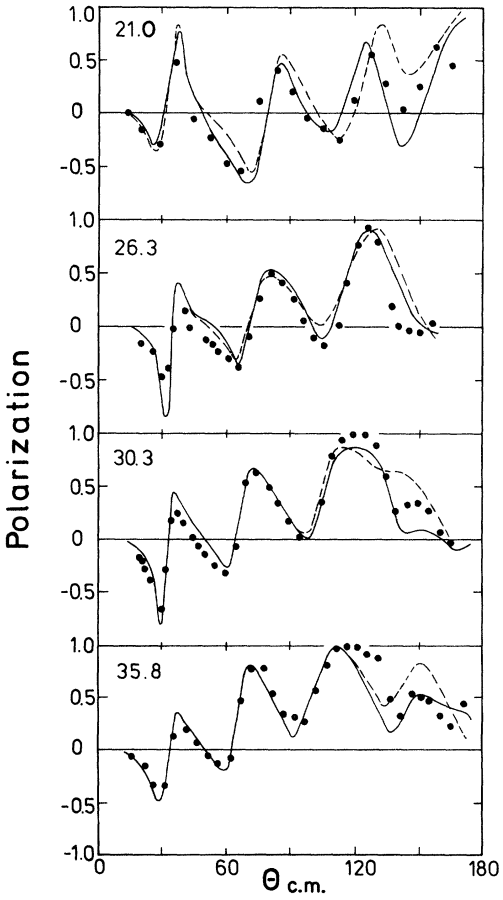

FIG. 6. ^{40}Ca polarization data and comparison with theoretical angular distributions with the same parameters as Fig. 5.

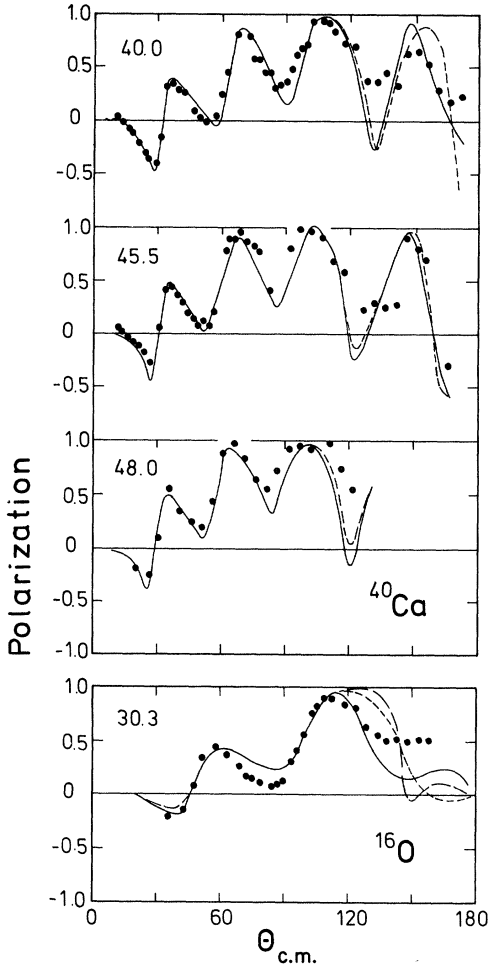

FIG. 7. Continuation of Fig. 6. In the lower part a similar comparison for ^{16}O is given.

In ^{40}Ar the quadrupole resonance is 0.5 MeV lower than in ^{40}Ca. Its width is larger, with 5–6 MeV instead of 3.5 MeV.[16-19] The strength is less certain, but probably lower in argon.[20] All these differences in $E2$ properties cause a lower effect in proton scattering. Actually ^{40}Ar displays elastic scattering cross sections with a backward peak which is less pronounced than for ^{40}Ca. Typical results of CC calculations are given in Fig. 8 at two incident energies. At 32.2 MeV the GQR is dominant, while at 40.7 MeV an octupole contribution is required, all similar to ^{40}Ca. To reproduce the splitting of the $E2$ resonance three 2^+ states have been positioned at 15.7, 18.5, and 21.3 MeV with a total strength of 55%. A 3^- state positioned at 35 MeV has been coupled with a strength of 15% EWSR. The average optical model potential set 4 of Table I has been used.

The other group of nuclei, which displays very large backward effects, consists of nitrogen and oxygen isotopes. All these nuclei display a GQR which is rather similar in energy, position, and width, with some change in the strength.[21] The backward peak in proton elastic scattering is large in ^{16}O and smaller in ^{18}O. Results of CC calculations are given here for these two nuclei. The kind of improvement obtained in comparison to OM calculations is shown in Fig. 8, at an incident energy around 30 MeV. This energy has been chosen because the analysis is less affected by ambiguities. In fact, the backward peak is not large below 25 MeV, but evident at 30 MeV and higher up to 50 MeV. However, data above 35 MeV can be reproduced by an OMP.[4] The ambiguities between OMP and collective couplings become large at higher energies. In the calculations of Fig. 8, a 2^+ state at 22 MeV has been coupled with the ground state. The strength is 70% and 60% of the EWSR limit for ^{16}O and ^{18}O, respectively. The potentials used are sets 5 and 6 of Table I. These potentials reproduce the known total reaction cross sections and polarization data,[22,23] both in OM and in CC calculations. Also for these two nuclei the CC calculations give a clear improvement in the agreement with the experiment. In Fig. 8 we compare the results of a best fit OM calculation on ^{16}O data.[4]

It should be noted, however, that the quality of fits for oxygen isotopes is less satisfactory than for ^{40}Ca or ^{40}Ar. The agreement cannot be improved by a more realistic description of the GQR or introducing other coupled states and cannot be improved even by refitting OM parameters if a reasonable agreement with both total reaction cross section and polarization data is required. This may be an indication that the coupling with GR can account for a part of the nuclear structure effects found in proton scattering at the closure of the $1p$ shell.

As mentioned above, a nuclear structure dependence of proton scattering is due to the spreading of the resonance. This becomes clear from nuclei such as Ne, Mg, or Si, whose GQR is known to have a very large width. In Fig. 9 results are shown of CC calculations for ^{24}Mg at an incident energy of 35.2 MeV. The three curves given in the upper part of the figure have been calculated by taking the quadrupole strength to be 60% of the

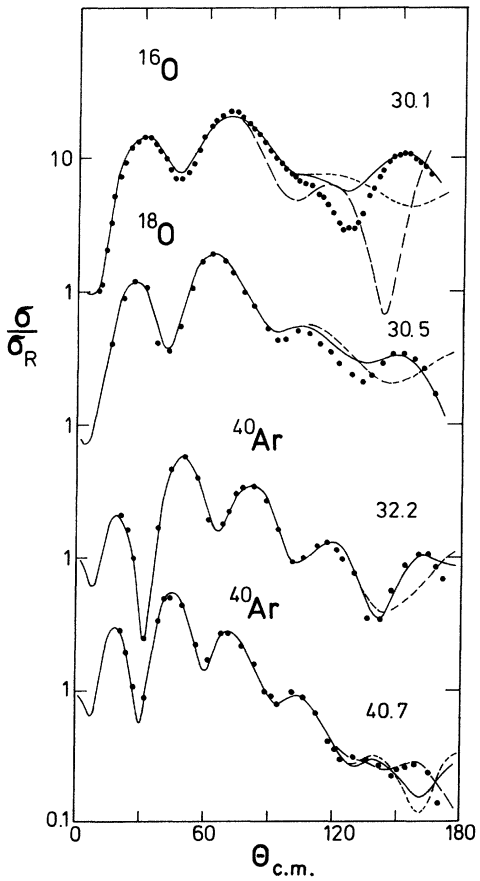

FIG. 8. Dashed curves are from OM calculations. Solid lines are from CC calculations in which the ground state is coupled to 2^+ GR states. The long-dashed curve gives for ^{16}O the result of a best fit OM calculation (Ref. 4), while for ^{40}Ar at 40.7 MeV the effect of an additional coupling with an octupole GR state is displayed.

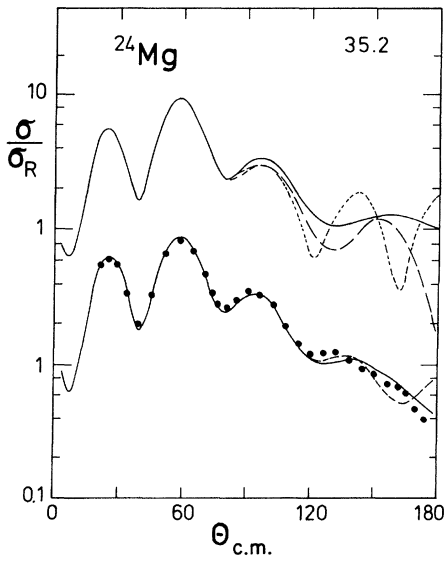

FIG. 9. The curves in the upper part are from CC calculations with a 2^+ state lying at 18, 24, and 30 MeV (solid, long-dashed, short-dashed lines). In the lower part experimental points are compared with OM calculations (dashed line) and CC calculations (solid line) with a strength distributed according to experiments (Ref. 24).

EWSR limit, concentrated in only one 2^+ state positioned at 18, 24, and 30 MeV, respectively. The backward maximum moves to forward angles when increasing the excitation energy of the coupled state. In the lower part, curves from OM calcuations (dashed line) and from CC calculations (solid line) are compared with experiment. In the latter calculation the $E2$ strength has been distributed over several 2^+ states positioned according to hadron scattering experiments.[24] The splitting of the resonance produces a smearing of the backward maximum. OM and CC calculations give different results especially in the angular region between 150°–180°. The very low values for the cross sections[2] found at 170° for nuclei such as ^{20,22}Ne and ^{24}Mg seem to come from the coupling of $E2$ states lying at 22–26 MeV excitation energy.

The spreading width of the resonance can also influence the effective strength needed in a simplified analysis. In the case of ^{40}Ca, RPA calculations predict a broad $E3$ resonance exhausting 30–70% of the EWSR limit.[18] The effect on proton scattering results is equivalent to taking a smaller strength concentrated, however, in only one 3^- state. From the present phenomenological analysis we conclude that differences in the spreading widths of GR, together with changes in the strengths, can account for nuclear structure effects found for light-medium weight nuclei in proton elastic scattering.

Finally a comparison of S-matrix elements shows that their modulus $|S_l|$ in CC calculations is systematically lower than in OM results. The difference is about 5–10%. The phases increase by 2°–6°. These changes are limited to low angular momenta up to the grazing partial wave. The collective coupling considered is therefore equivalent to l-dependent optical potentials, both repulsive and absorptive.[10]

IV. CONCLUSIONS

Back angle deficiencies in proton elastic scattering cross sections, occurring in OM calculations, are explained with the coupling of the ground state and high-lying states clustered in the giant resonance region. The strength needed to reproduce proton scattering data is consistent with depletions of the EWSR limit as predicted in RPA calculations or seen in hadron scattering experiments. Structure effects found for $1p$- and $1d$- shell nuclei are connected with changes in the structure of giant resonances and thereby mainly with their spreading widths.

The introduction of these collective couplings does not require readjustments of average OM parameters despite a small reduction (0.1–0.2 MeV) in the strength of the imaginary part. The inelastic channels considered here are nearly closed channels, with a small cross section. These channels give sizable reflection in the elastic channel and affect the angular structure of the elastic cross sections more than strong inelastic transitions to low-lying collective states.

No need for the inclusion of reaction channels, such as the deuteron channel, has been found for medium-mass nuclei. This conclusion is maintained even though we did not fit, as shown in Sec. III, $1p$-shell nuclei very satisfactorily. But in this case small inadequacies in OM potentials or in the model assumed for the process cannot be ruled out.

The analysis reveals that giant resonance channels are equivalent to effective l-dependent absorptive and repulsive optical model potentials. The need for unification of the Brueckner-Hartree-Fock potential with the nuclear structure approach of the microscopic OM potentials, as discussed in Sec. II, is clearly established.

As a final comment it appears useful to refer to older investigations of inelastic proton scattering in similar energy regions.[25] In these studies nonnormal parity transitions or charge exchange transitions were chosen. This choice was made to combine particular features of the effective interaction with simple transition density structures in order to enhance the importance of giant resonances as intermediate states. The present treatment is not unrelated as both calculations use collective transition form factors to the giant multipole states with a strength extracted from or comparable with direct excitation information.

This work was supported by the Bundesministerium für Forschung und Technologie under Contract No. 06HH726.

---

*Permanent address: Istituto di Fisica dell'Universita' di Milano, Milano, Italy.

[1]E. Fabrici, S. Micheletti, M. Pignanelli, F. G. Resmini, R. De Leo, G. D'Eraso, A. Pantaleo, J. L. Escudié, and A. Tarrats, Phys. Rev. C 21, 830 (1980).

[2]E. Fabrici, S. Micheletti, M. Pignanelli, F. G. Resmini, R. De Leo, G. D'Erasmo, and A. Pantaleo, Phys. Rev. C 21, 844 (1980).

[3]E. E. Gross, R. H. Bassell, L. N. Blumberg, B. J. Morton, A. van der Woude, and A. Zucker, Nucl. Phys. A102, 673 (1969).

[4]W. T. H. van Oers and J. M. Cameron, Phys. Rev. 184, 1061 (1969).

[5]W. T. H. van Oers, Phys. Rev. C 3, 1550 (1971).

[6]J. P. Jeukenne, A. Lejeune, and C. Mahaux, Phys. Rep. 25C, 83 (1976); Phys. Rev. C 16, 80 (1977); A. Lejeune and P. E. Hodgson, Nucl. Phys. A295, 301 (1978).
[7]F. A. Brieva and R. J. Rook, Nucl. Phys. A291, 299 (1977); A291, 317 (1977); A297, 206 (1978); A307, 493 (1978).
[8]H. P. Gubler, U. Kiebele, H. O. Meyer, G. R. Plattner, and I. Sick, Phys. Lett. 74B, 202 (1978).
[9]R. S. Mackintosh and L. Cordero, Phys. Lett. 68B, 323 (1977).
[10]A. M. Kobos and R. S. Mackintosh, J. Phys. G 5, 97 (1979); 5, 359 (1979).
[11]R. S. Mackintosh, Nucl. Phys. A230, 195 (1974); R. S. Mackintosh and A. M. Kobos, Phys. Lett. 62B, 127 (1977).
[12]N. Vinh Mau and A. Bouyssy, Nucl. Phys. A257, 189 (1976).
[13]N. Vinh Mau, *Microscopic Optical Potentials*, Lecture Notes in Physics, edited by H. V. von Geramb (Springer, New York, 1979), Vol. 89, p. 40.
[14]P. W. Coulter and G. R. Satchler, Nucl. Phys. A293, 269 (1977).
[15]H. V. von Geramb, F. A. Brieva, and R. J. Rook, *Microscopic Optical Potentials*, Lecture Notes in Physics, edited by H. V. von Geramb (Springer, New York, 1979), Vol. 89, p. 104.
[16]F. E. Bertrand, Annu. Rev. Nucl. Sci. 26, 457 (1976).
[17]F. E. Bertrand, G. R. Satchler, D. J. Horen, and A. van der Woude, Phys. Lett. 80B, 198 (1979).
[18]S. Krewald, J. Birkholz, A. Faessler, and J. Speth, Phys. Rev. Lett. 33, 1386 (1974); K. F. Liu and G. E. Brown, Nucl. Phys. A265, 385 (1976).
[19]J. P. Didelez, C. Mayer-Böricke, W. O. Oelert, M. Rogge, P. Turek, and S. Wiktor, Nucl. Phys. A318, 205 (1979).
[20]D. H. Youngblood, J. M. Moss, C. M. Rozsa, J. D. Bronson, A. D. Bacher, and D. R. Brown, Phys. Rev. C 13, 994 (1976).
[21]K. T. Knöpfle, C. Meyer-Böricke, W. Oelert, H. Riedesel, M. Rogge, and G. J. Wagner, Annual Report No. KFA-IKP, Julich, 1976, p. 5; G. J. Wagner, *Nuclear Interactions*, Lecture Notes in Physics, edited by B. A. Robson (Springer, New York, 1979), Vol. 92, p. 269.
[22]R. F. Carlson, A. J. Cox, J. R. Nimmo, N. E. Davison, S. A. Elbakr, J. L. Horton, A. Houdayer, A. M. Sourkes, W. T. H. van Oers, and D. J. Margaziotis, Phys. Rev. C 12, 1167 (1975).
[23]R. De Swiniarski, F. G. Resmini, D. L. Hendrie, and A. D. Bacher, Nucl. Phys. A261, 111 (1976).
[24]D. H. Youngblood, C. M. Rozsa, J. M. Moss, D. R. Brown, and J. D. Bronson, Phys. Rev. C 15, 1644 (1977); T. S. Bauer, R. Beurtey, A. Boudard, G. Brouge, H. Catz, P. Couvert, J. L. Escudié, J. M. Fontaine, M. Garson, J. C. Lugol, M. Motoba, S. Platchkov, M. Rouger, and Y. Terrien, *ibid.* 19, 1438 (1979).
[25]H. V. Geramb, R. Sprickmann, and G. L. Strobel, Nucl. Phys. A199, 545 (1973).